nature geoscience

SUPPLEMENTARY INFORMATION

DOI: 10.1038/NGEO1671

Central West Antarctica among most rapidly warming regions on Earth

Supplementary Information

This file contains:

1 Supplementary Discussion

1.1 Byrd 1980s warming and atmospheric circulation over the Ross-Amundsen Seas

We found the rapid 1980s warming at Byrd in DJF to coincide with a change in the position of the persistent center of low pressure off the coast of West Antarctica (Supplementary Fig. S5). Often termed Amundsen-Sea low[1], it resides predominantly over the Ross Sea in the non-summer months and tends to migrate towards the Bellingshausen Sea during austral summer[2]. The variability of its position is markedly greater in DJF than during the rest of year, which is apparent in the time-averaged geopotential height field (Supplementary Fig. S5a). A low positioned in the Ross Sea favors greater meridional heat transport toward Marie Byrd Land, and therefore warmer conditions at Byrd[3]. A transition occurred in 1989 when the low started residing predominantly in the Ross Sea in DJF, until roughly the mid-1990s (Supplementary Fig. S5b). This transition coincided with the SAM starting to shift toward its high polarity and with a slight increase (6%) in the number of cyclones in the broad Amundsen-Bellingshausen Sea region[4]. Surprisingly, further (and sharper) increase in the SAM index in the mid-1990s did not have any clear effect on the position of the low. Moreover, this position has not displayed any significant longitudinal trend in DJF since 1979 (ref. 1; Supplementary Fig. S5b). As a result, this mechanism *alone* is unlikely to account for the long-term summer warming. This issue deserves further investigation beyond the scope of this paper.

2 Supplementary Methods

2.1 Background on the temperature observations from Byrd Station/AWS

2.1.1 Historical background

The first occupied Byrd Station was established in January 1957 as a year-round research facility. In February 1962, a second station ("New Byrd") was commissioned, 10 km from the original site ("Old Byrd", abandoned) and slightly higher in elevation (1533 m versus 1511 m) (refs 5, 6). Old and New Byrd provided uninterrupted near-surface temperature observations from 1957 to 1969. In the early 1970s, the facility transitioned into a summer-only station, known as Byrd Surface Camp (BSC), which has since been occupied intermittently during the Antarctic field season. Aiming to continue the existing temperature record, a redesigned Stanford AWS was installed in 1979, 1.4 km from BSC, 1530 m a.s.l., with the qualified Byrd AWS data record beginning as of January 1980 (refs 7, 8). Since then, the AWS has been maintained by the Antarctic Meteorological Research Center (AMRC) at the University of

Wisconsin-Madison, as part of the U.S. Antarctic AWS Program[8]. A GPS survey of the area[9] carried out in the early 2000s did not suggest any significant change in the AWS elevation since 1980. The proximity of the successive locations and the small elevation differences between them suggest little impact of the moving of the measurement site on the long-term temperature trends.
The challenges of operating autonomous systems in the Antarctic (long polar night, harsh climate, limited window for maintenance during austral summer) have resulted in numerous interruptions in the AWS observations. Their remarkable continuity through most of the 1980s is attributed to the radioisotope thermoelectric generator (RTG) originally used as a power source for the AWS[8]. The RTG was subsequently replaced with batteries charged (only during the polar day) by solar panels, making the AWS more prone to power outages, particularly during austral winter and spring.

2.1.2 Corrections to Byrd AWS observations from 1989–01/2011

On 18 January 2011, a new CR1000 datalogger (used to record and disseminate the readings from the various AWS sensors) was installed on the Byrd AWS in replacement of the AWS-2B electronic system used since 1989. Upon inspection of the old system at the AMRC, a calibration error of 1.5 °C (in excess) was identified for the temperature observations recorded since 2002. In addition, subsequent testing in a newly available cold chamber at the AMRC provided more accurate measurements of the temperature sensitivity of the AWS-2B system, which results in a negative temperature drift as the temperature decreases. As a result, corrections were made to the temperature observations recorded by the Byrd AWS between 1989 and 17 January 2011. The release of the corrected dataset on the AMRC's ftp server in December 2011 was followed by an update of the monthly mean temperatures from Byrd AWS available on the READER online archive[10] (http://www.antarctica.ac.uk/met/READER/).
The effect of the corrections on the reconstructed temperatures is illustrated in Supplementary Fig. S10. In the lower temperature range (typically -50 to -30 °C), the temperature drift largely compensated for the 1.5 °C error in the 2002–01/2011 observations, whereas no compensation occurred at higher temperatures (-20 to 0 °C). This explains the differences in the corrections' impact between summer and winter, and between the 1989-2001 and 2002-2010 periods (Supplementary Fig. S10). It is noteworthy that the temperature drift problem did not affect significantly the AWS observations from 1980–1988, and this for two reasons: (1) Excess power from the RTG was used to keep the internal temperature of the electronics above -20 °C. This extra power was no longer available when the AWS started relying on batteries charged by solar panels. (2) The central processing unit of the AWS was (paradoxically) a newer version than the one subsequently used from 1989 onward.

2.1.3 Potential sources of error in the AWS observations

Could the observations from Byrd be in error and overestimate the long-term temperature increase, especially during summer? One possible source of error comes from the non-adjustment of the temperatures to height changes due to snow accumulation. This is an important issue because of the strong surface temperature inversion characteristic of the Antarctic boundary layer[11]. The main reason why this problem is likely inconsequential here is that it would actually cause the observations to *underestimate* the temperatures compared to a properly calibrated record. In addition, the sensors are periodically raised on the AWS mast during maintenance visits.

A second concern has been suggested by a recent study[12] showing AWS temperature measurements in the East Antarctic interior to be likely biased warm in summer because of intense solar radiation and insufficient ventilation of the sensor, particularly during low-wind conditions. Again, several lines of evidence suggest that this problem does not affect the Byrd observations: (1) During summer, the near-surface wind speed at Byrd is typically 1.5 times higher than on the adjacent East Antarctic plateau (based upon monthly mean wind speeds from the READER archive[10]). (2) Cloudiness is greater at Byrd Station[13], reducing the amount of incoming solar radiation at the surface. (3) The occurrence of warmer-than-normal summer months in the 1990s and 2000s was corroborated by surface melt episodes in the vicinity of Byrd[14], most notably in January 2005 (ref. 15). (4) Finally, the marked increase in the mean summer temperature at Byrd during the 1980s is consistent with changes in the atmospheric circulation, as shown in Supplementary Figs S5 and S6.

2.2 Details on the infilling method

2.2.1 Infilling of the Byrd record: 1979–2011 period (alternative method)

The Methods section of the main text describes the procedure used to fill in the Byrd record for months without *any* observations. A variant of the method is used when observations are *partially* available during a given month. In this case, the infilling relies upon 6-hourly temperature observations from the AWS (resampled from the 3-hourly data obtained from the AMRC ftp server); and ERA-Interim[16] (ERA-I) 6-hourly T_{2m} data (here again, the reanalysis data are from the short-term forecast fields). The reconstructed monthly mean temperature at Byrd (T_{rec}) is estimated, for each month, by (1) computing the difference (ΔT) between all available 6-hourly AWS observations and the corresponding 6-hourly T_{2m} data from ERA-I; and (2) using ΔT to adjust ERA-I monthly mean T_{2m}. Unsurprisingly, the error of T_{rec} increases as the percentage of observations available per month decreases (Supplementary Fig. S11). In other words, the fewer the observations available, the less ΔT becomes representative of the ERA-I temperature bias for the entire month. The cut-off percentage for this adjustment method to be used is set to 40% as it ensures RMSE $\leq$1 °C (Supplementary Fig. S11). This alternative method is used only for a small percentage (11%) of the months with

incomplete/missing observations during 1979–2011 (126 in total). It is primarily designed to take advantage of the few spring months with observations during the late 1990s and 2000s.

2.2.2 ERA-Interim forecast versus analysis temperatures

When using ERA-I T_{2m} estimates, one caveat arises from the use of temperature observations from Byrd AWS in the reanalysis itself through its data assimilation system[16,17]. While this forces the reanalysis model to remain close to the observations, it also leads to an underestimation of the model error in the absence of observations, i.e., precisely when ERA-I data are needed for our temperature reconstruction. As a result, we used ERA-I *forecast* T_{2m} data, which are produced by the reanalysis model short-term forecasts, rather than ERA-I *analysis* T_{2m} data, which result from the combination of the short-term forecast fields (a.k.a. background or "first-guess" fields) with all available observations. The forecast T_{2m} time series are constructed from the 6th and 12th hours of the forecasts initialized at 0000 UTC and 1200 UTC. The difference between analysis and forecast T_{2m} denotes the impact of the observations, and thus the reanalysis model bias.
One additional feature of ERA-I T_{2m} is of particular interest for our purpose. In ERA-I, the assimilation of near-surface temperatures is performed separately from the main (4D-Var) assimilation system, using an Optimal Interpolation (OI) scheme[16,18]. Further, the analysis T_{2m} generated by the OI is not used to modify the temperature field which is carried on to initialize the short-term forecasts[18]. In other words, ERA-I forecast T_{2m} estimates at Byrd are not affected by the AWS observations, even when these are available. This condition of independence between model estimates and observations is essential for estimating, and correcting for, the "true" reanalysis bias in our infilling method. As one would expect, the RMSE of ERA-I forecast T_{2m} (1.27 °C) is greater than that of the analysis T_{2m} (1.01 °C). However, this difference is small, and the forecast T_{2m} RMSE is substantially lower for ERA-I than for the other reanalyses (Supplementary Fig. S8).

2.3 Uncertainty calculation

2.3.1 Uncertainties of the reconstructed temperatures

The uncertainties of our temperature reconstruction are assessed separately for the 1970-1978 and 1979-2011 periods. For 1979-2011, monthly mean temperatures (T_{rec}) predicted by our ERA-I-based infilling method can be directly compared against AWS observations. As shown in Supplementary Fig. S9a, the T_{rec} estimates from 1979-2011 are characterized by an RMSE of 0.87 °C. The smallness of the RMSE can be appreciated when compared against the standard deviations of the monthly temperatures at Byrd (Supplementary Fig. S9d). The biases of T_{rec} with respect to the observations do not exhibit any particular temperature dependence. Their relatively uniform distribution around zero (Supplementary Fig. S9c) explains the negligible overall bias (0.01 °C). This also results in a smaller RMSE (0.62 °C) for the mean

seasonal temperatures (Supplementary Fig. S9b). It must be noted that the derivation of such RMSE statistics is possible because the temporal gaps in the observations are limited in extent and the skill of ERA-I relatively homogeneous throughout the period.
Such conditions are not verified during the 1970-1978 period. Indeed, with the exception of a few summer months, temperature observations are completely absent during this time interval (see main text Fig. 2, histograms). In addition, the quality of the reanalyses (ERA-40, NNR) is highly variable in time. It increases most significantly with the introduction of abundant satellite observations in 1979 (ref. 19). Thus, meaningful RMSE statistics cannot be derived for this period. As a result, the envelope of uncertainties around T_{rec} is defined by the two temperature curves generated with the two infilling methods employed for this portion of the Byrd record (see section above). For each month without observations, the error of T_{rec} is taken as half the difference between the temperature estimates suggested by the two methods. As shown in table S1, the temperatures from 1970–1978 have a minimal impact on the 1958–2010 temperatures trends.

2.3.2 Uncertainties of the temperature trends

The uncertainties of the temperature trends referred to in the main text and given in main text Fig. 3a,b, Supplementary Table S1, and (for our reconstruction only) Supplementary Table S2 include both the standard errors of the regressions and the uncertainties of the infilling methods. For the standard error, the sample size, n, used is adjusted for autocorrelations in the time series as described in ref. 20. The resulting effective sample size, n_{eff}, is defined as $n_{eff} = n(1 - r_1)/(1 + r_1)$, where r_1 is the lag-1 autocorrelation.
The trend uncertainties due to the infilling are estimated via a Monte Carlo procedure[21]. A large number ($N = 10^5$) of realizations of our temperature reconstruction are generated by randomly varying the temperature estimates within plus or minus two RMSE around T_{rec} for months without observations (for 1970-1978, temperatures are randomly selected within twice the range of uncertainties defined above). The linear trends that are derived from each realization are normally distributed around a mean trend value. The uncertainties of the trends for the monthly, seasonal and annual mean temperatures are taken as two standard deviations of the respective normal distributions. Note that this second type of uncertainty is one order of magnitude smaller than the standard errors of the regressions.

3 Supplementary Material

3.1 Global reanalysis data

The ERA-I and ERA-40 data are obtained from the ECMWF data server (http://data-portal.ecmwf.int/). Note that the ERA-I data at full resolution ($\sim$0.7 $^\circ$ in latitude-longitude) are used in for our reconstruction. The NCEP-NCAR data are obtained

from NOAA's NOMADS server (http://nomad3.ncep.noaa.gov/ncep_data/). The two additional reanalysis datasets used in Supplementary Fig. S8 are NASA's Modern Era Retrospective-analysis for Research and Applications[22] (MERRA), and NCEP's Climate Forecast System Reanalysis[23] (CFSR). The MERRA data are obtained from NASA's MDISC data portal (http://disc.sci.gsfc.nasa.gov/daac-bin/DataHoldings.pl). The CFSR data are obtained from NCAR's Research Data Archive (http://dss.ucar.edu/pub/cfsr.html).

3.2 Global temperature data

The global temperature estimates used in main text Fig. 3c are from the CRUTEM4 dataset produced by the University of East Anglia Climatic Research Unit and available at http://www.cru.uea.ac.uk/cru/data/temperature/.

4 References

1. Turner, J., Phillips, T., Hosking, J. S., Marshall, G. J. & Orr, A. The Amundsen Sea low. *Int. J. Climatol.* doi:10.1002/joc.3558 (published online 15 Aug. 2012).

2. Bromwich, D. H. & Wang, S.-H. A review of the temporal and spatial variability of Arctic and Antarctic atmospheric circulations based upon ERA-40. *Dyn. Atmos. and Oceans* **44**, 213–243 (2008).

3. Nicolas, J. P. & Bromwich, D. H. Climate of West Antarctica and influence of marine air intrusions. *J. Climate* **24**, 49–67 (2011).

4. Fogt, R. L., Wovrosh, A. J., Langen, R. A. & Simmonds, I. The characteristic variability and connection to the underlying synoptic activity of the Amundsen-Bellingshausen Seas low. *J. Geophys. Res.* **117**, D07111 (2012).

5. Schwerdtfeger, W. The climate of the Antarctic. In Orvig, S. (ed.) *Climates of the Polar Regions*, vol. 14 of *World Survey of Climatology*, chap. 4, 253–355 (Elsevier, 1970).

6. Stewart, A. *Antarctica: An Encyclopedia* (McFarland and Co., London, 1990).

7. Stearns, C. R. & Savage, M. L. Automatic weather stations: 1980-1981. *Ant. J. US* **16**, 190–192 (1981).

8. Lazzara, M. A., Weidner, G. A., Keller, L. M., Thom, J. E. & Cassano, J. J. Antarctic Automatic Weather Station Program: 30 years of polar observations. *Bull. Amer. Meteor. Soc.* **93**, 1519–1537 (2012).

9. Hamilton, G. S. & Spikes, V. B. Evaluating a satellite altimeter-derived digital elevation model of Antarctica using precision kinematic GPS profiling. *Global and Planetary Change* **42**, 17–30 (2004).

10. Turner, J. *et al.* The SCAR READER project: Toward a high-quality database of mean Antarctic meteorological observations. *J. Climate* **17**, 2890–2898 (2004).

11. Ma, Y. F., Bian, L. G. & Xiao, C. D. Impacts of snow accumulation on air temperature measured by automatic weather stations on the Antarctic ice sheet. *Adv. Polar. Sci.* **22**, 17–24 (2011).

12. Genthon, C., Six, D., Favier, V., Lazzara, M. & Keller, L. Atmospheric temperature measurement biases on the Antarctic Plateau. *J. Atmos. Oceanic Technol.* **28**, 1598–1605 (2011).

13. Turner, J. & Pendlebury, S. (eds.) *The International Antarctic Weather Forecasting Handbook* (British Antarctic Survey, Cambridge, UK, 2004).

14. Tedesco, M., Abdalati, W. & Zwally, H. J. Persistent surface snowmelt over Antarctica (1987-2006) from 19.35 GHz brightness temperatures. *Geophys. Res. Lett.* **34**, L18504 (2007).

15. Nghiem, S. V., Steffen, K., Neumann, G. & Huff, R. Snow accumulation and snowmelt monitoring in Greenland and Antarctica. In Tregoning, P. & Rizos, C. (eds.) *Dynamic planet: monitoring and understanding a dynamic planet with geodetic and oceanographic tools, IAG Symp., Cairns, Australia 22-26 Aug. 2005*, 31–38 (2005).

16. Dee, D. P. *et al.* The ERA-Interim reanalysis: configuration and performance of the data assimilation system. *Quart. J. Roy. Meteor. Soc.* **137**, 553–597 (2011).

17. Uppala, S. M. *et al.* The ERA-40 re-analysis. *Quart. J. Roy. Meteor. Soc.* **131**, 2961–3012 (2005).

18. Simmons, A. J., Willett, K. M., Jones, P. D., Thorne, P. W. & Dee, D. P. Low-frequency variations in surface atmospheric humidity, temperature, and precipitation: Inferences from reanalyses and monthly gridded observational data sets. *J. Geophys. Res.* **115**, D01110 (2010).

19. Bromwich, D. H. & Fogt, R. L. Strong trends in the skill of the ERA-40 and NCEP-NCAR reanalyses in the high and middle latitudes of the Southern Hemisphere, 1958-2001. *J. Climate* **17**, 4603–4619 (2004).

20. Santer, B. D. *et al.* Statistical significance of trends and trend differences in layer-average atmospheric temperature time series. *J. Geophys. Res.* **105**, 7337–7356 (2000).

21. Von Storch, H. & Zwiers, F. W. *Statistical Analysis in Climate Research* (Cambridge University Press, 1999).

22. Rienecker, M. M. *et al.* MERRA: NASA's Modern-Era Retrospective Analysis for Research and Applications. *J. Climate* **24**, 3624–3648 (2011).

23. Saha, S. *et al.* The NCEP Climate Forecast System Reanalysis. *Bull. Amer. Meteor. Soc.* **91**, 1015–1057 (2010).

24. Picard, G. & Fily, M. Surface melting observations in Antarctica by microwave radiometers: Correcting 26-year time series from changes in acquisition hours. *Remote Sens. Environ.* **104**, 325–336 (2006).

25. Ding, Q., Steig, E. J., Battisti, D. S. & Kuttel, M. Winter warming in West Antarctica caused by central tropical Pacific warming. *Nature Geosci.* **4**, 398–403 (2011).

26. Ding, Q., Steig, E. J., Battisti, D. S. & Wallace, J. M. Influence of the tropics on the Southern Annular Mode. *J. Climate* **25**, 6330–6348 (2012).

27. Chapman, W. L. & Walsh, J. E. A synthesis of Antarctic temperatures. *J. Climate* **20**, 4096–4117 (2007).

28. Monaghan, A. J., Bromwich, D. H., Chapman, W. & Comiso, J. C. Recent variability and trends of Antarctic near-surface temperature. *J. Geophys. Res.* **113**, D04105 (2008).

29. Steig, E. J. *et al.* Warming of the Antarctic ice-sheet surface since the 1957 International Geophysical Year. *Nature* **457**, 459–462 (2009).

30. O'Donnell, R., Lewis, N., McIntyre, S. & Condon, J. Improved methods for PCA-based reconstructions: Case study using the Steig et al. (2009) Antarctic temperature reconstruction. *J. Climate* **24**, 2099–2115 (2010).

31. Küttel, M., Steig, E. J., Ding, Q., Monaghan, A. J. & Battisti, D. S. Seasonal climate information preserved in West Antarctic ice core water isotopes: relationships to temperature, large-scale circulation, and sea ice. *Climate Dyn.* **39**, 1841–1857 (2012).

5 Supplementary Figures

5.1 Figures related to the main text discussion

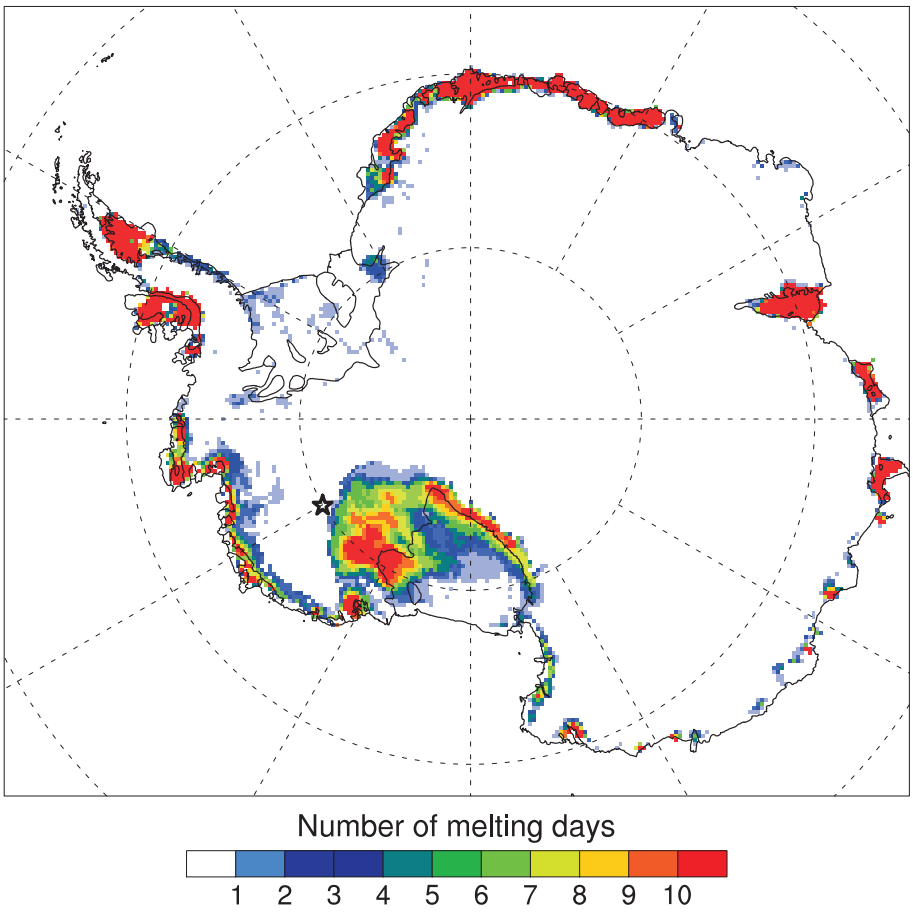

Supplementary Figure S1 | Number of melting days over Antarctica in January 2005 as detected by satellite passive microwave observations (SSM/I). The black star identifies the location of Byrd Station. The data are courtesy of G. Picard and available at http://www-lgge.obs.ujf-grenoble.fr/~picard/melting/. Additional details can be found in Picard and Fily (2006) [ref. 24].

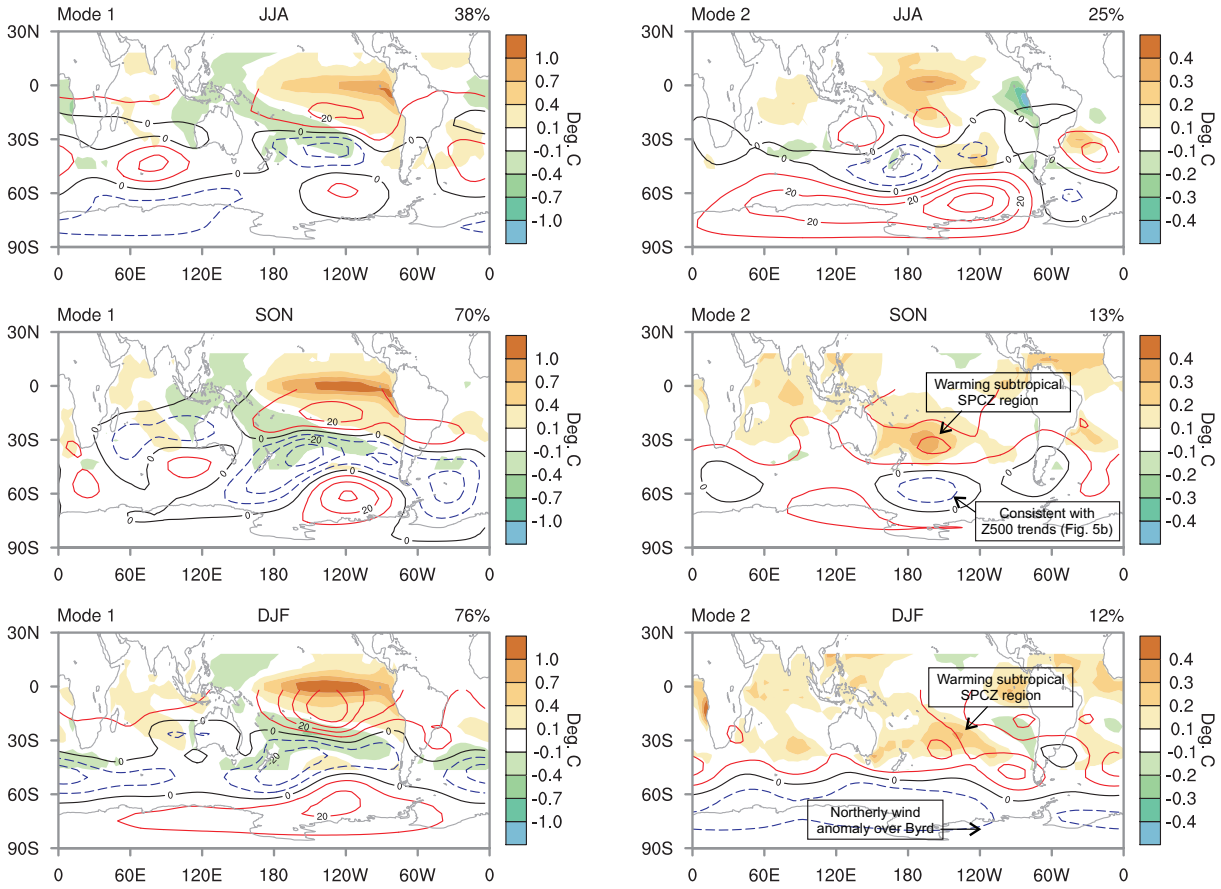

Supplementary Figure S2 | Maximum covariance analysis (MCA) between sea surface temperature (SST) and 200 hPa geopotential height (Z200) for 1979–2009. The MCA is done as in Ding *et al.* (2011, 2012) [refs 25 and 26], only with SST 50 °S to 20 °N (instead of 20 °S to 20 °N) and Z200 data from ERA-Interim (instead of a composite ERA-40/ERA-Interim). The figure shows the spatial patterns of SST (50 °S to 20 °N) and Z200 (equator to 87.5 °S) associated with the first (left column) and second (right) modes of covariability between these two fields. The number in the upper-right corner indicates the percent covariance explained by each mode. As in Ding *et al.* (2011), the amplitudes are scaled by one standard deviation of their respective time series, which are shown in Supplementary Fig. S3. Units are degrees Celsius for SST and meters for Z200. The SST data are from the Extended Reconstructed Sea Surface Temperature (ERSST) version 3, available at http://www.ncdc.noaa.gov/ersst/.

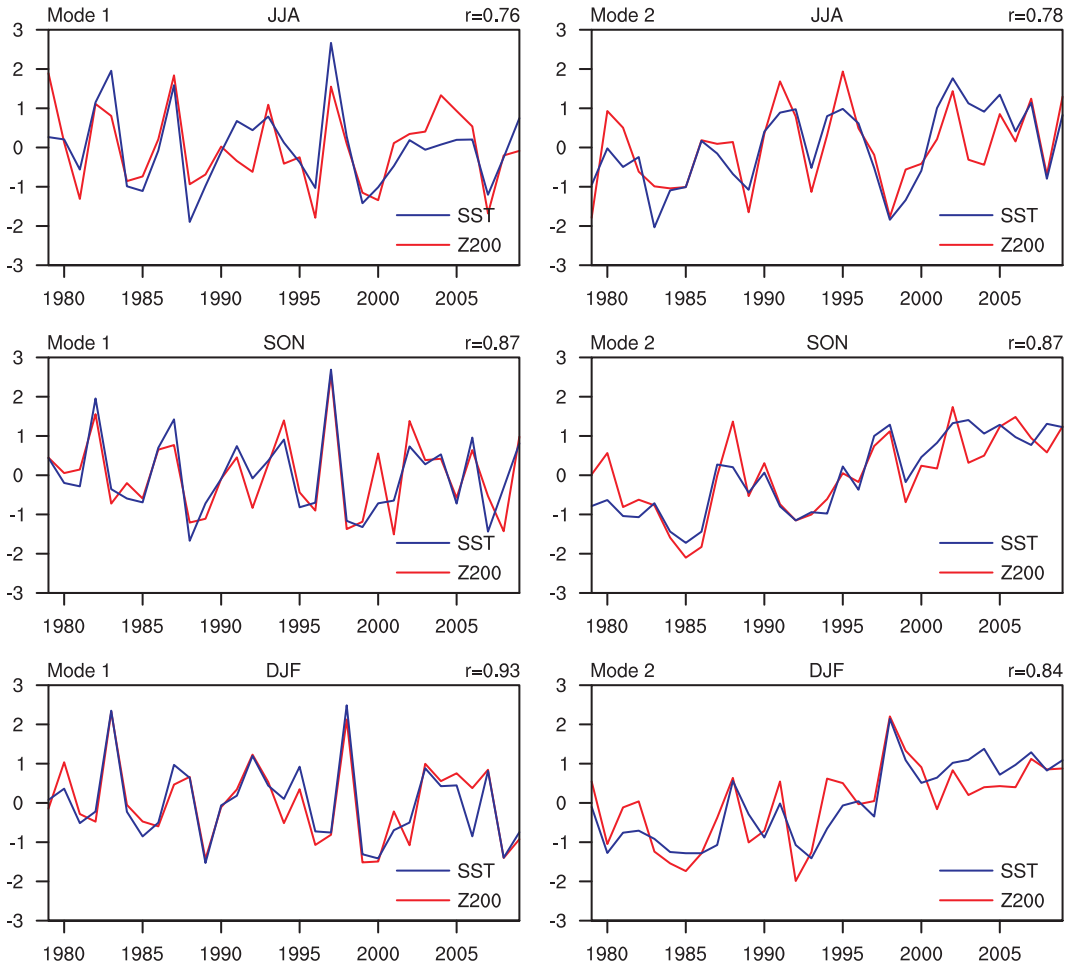

Supplementary Figure S3 | Maximum covariance analysis between sea surface temperature (SST) and 200 hPa geopotential height (Z200) for 1979–2009. The figure shows the expansion coefficients of the first and second modes (the patterns are shown in Supplementary Fig S2). The number in the upper-right corner indicates the correlation between the SST and Z200 time series.

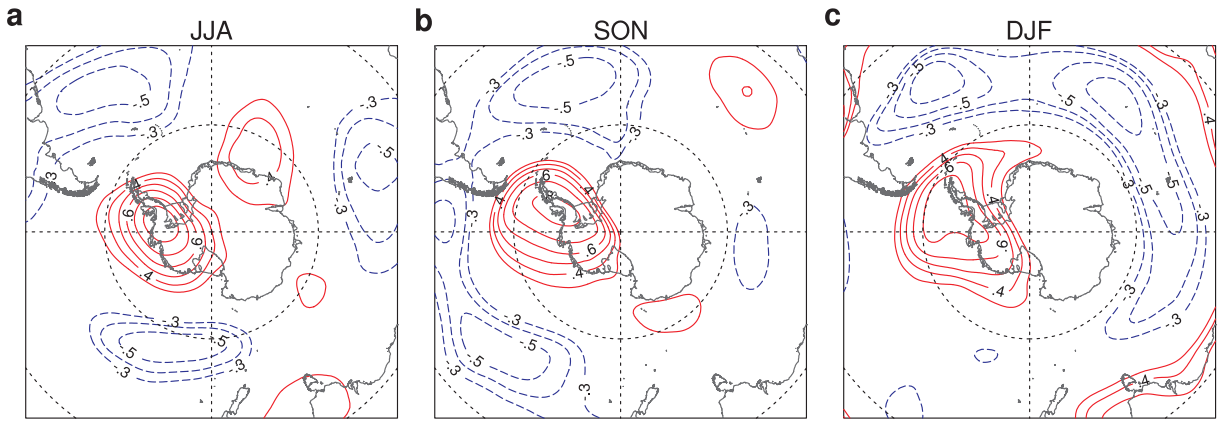

Supplementary Figure S4 | Correlations between Byrd temperatures and ERA-Interim 500 hPa geopotential height calculated for 1989–2011 during the three warming seasons: winter (JJA), spring (SON), and summer (DJF). The correlations are calculated with detrended time series.

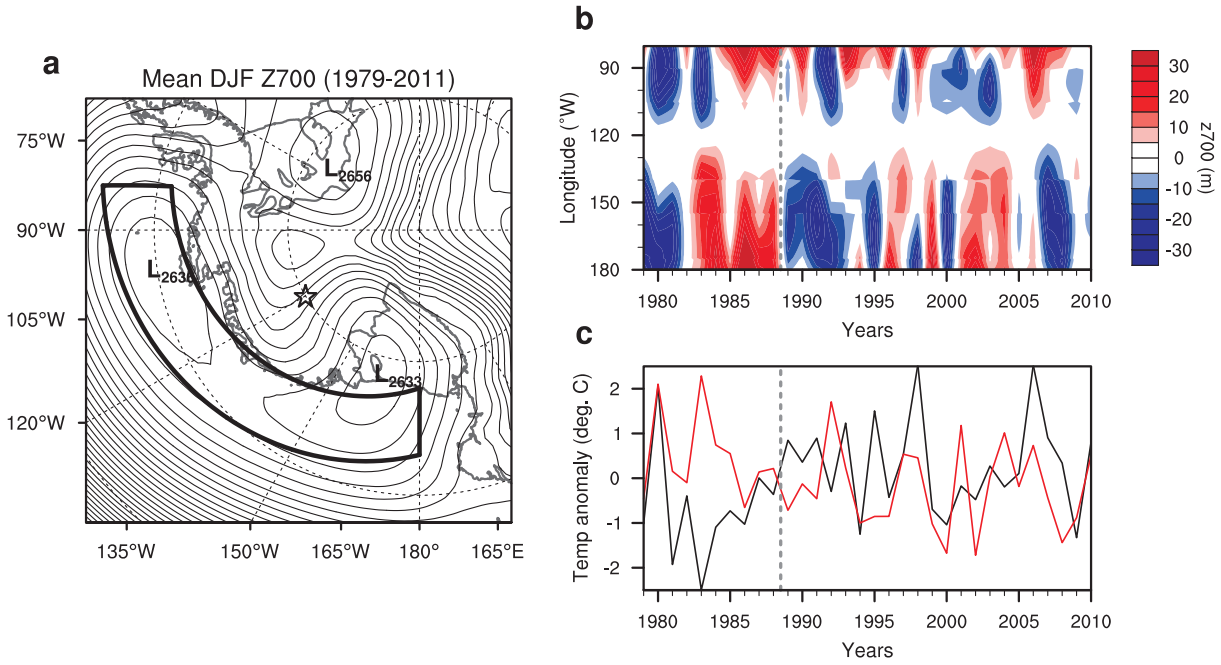

Supplementary Figure S5 | **a**, Time-averaged 700 hPa geopotential height (Z700) field in DJF during 1979–2011. The star symbol denotes the location of Byrd. **b**, Hovmueller diagram showing the difference in Z700 relative to longitude 120 °W as a function of the longitude (y-axis) and time (x-axis). The Z700 field is meridionally averaged over the area shown with a black box in **a**. **c**, Temperature anomalies at Byrd in DJF. The dashed gray line in **b** and **c** highlights the marked temperature increase at Byrd in the late 1980s.

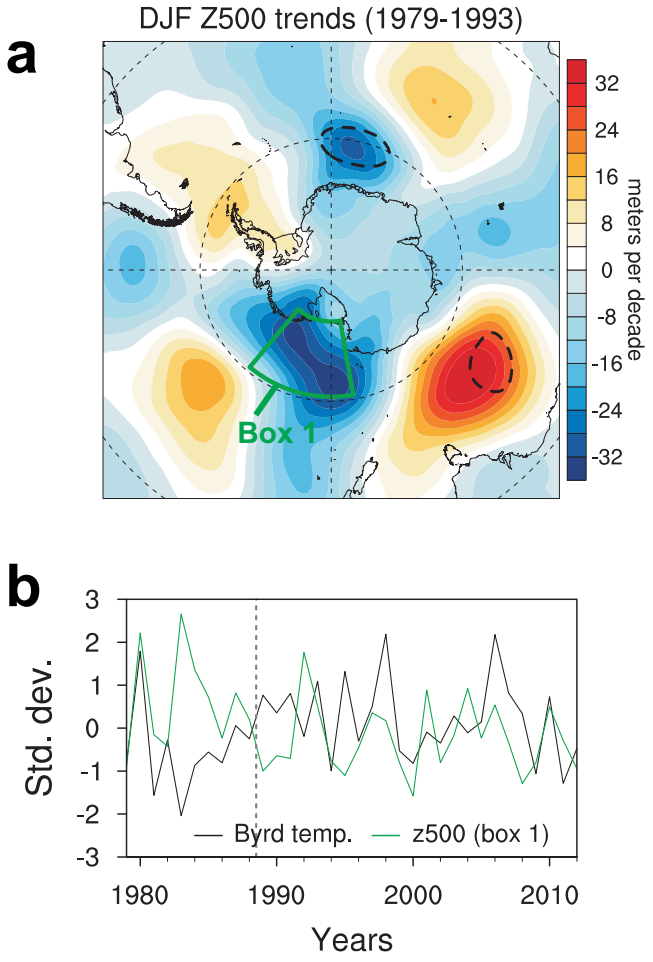

Supplementary Figure S6 | (Top) Linear trends in ERA-Interim 500 hPa geopotential height in austral summer (DJF) during 1979–1993. The thick black dashed lines denotes the 95% significance level of the trends. (Bottom) Times series of mean DJF temperature at Byrd (black line) and Z500 averaged over the Ross Sea ('Box 1'). As in Supplementary Fig. S5, the dashed gray line highlights the marked temperature increase at Byrd in the late 1980s.

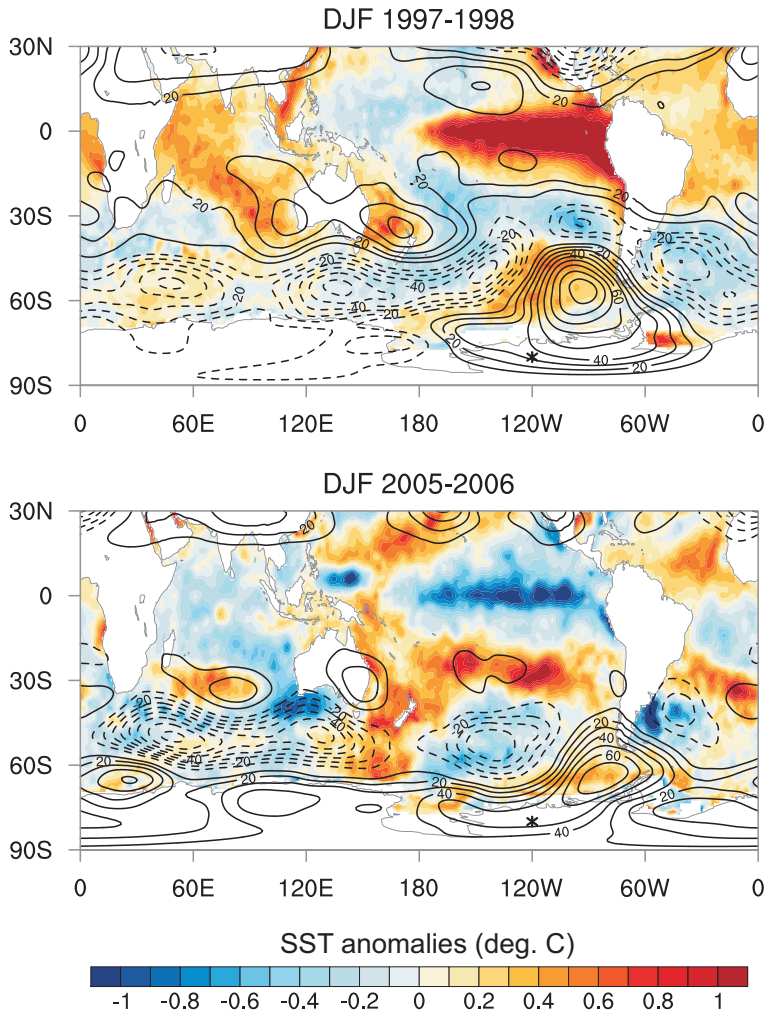

Supplementary Figure S7 | Sea surface temperature (SST) and 500 hPa geopotential height (Z500) anomalies in austral summer 1997-1998 (top) and 2005-2006 (bottom). These two summers were the two warmest at Byrd since 1957 (see main text Fig. 2). SST anomalies, in degrees Celsius, are color-shaded. Z500 anomalies, in meters, are shown with black line contours. The black star symbol denotes the location of Byrd.

5.2 Figures related to the infilling method

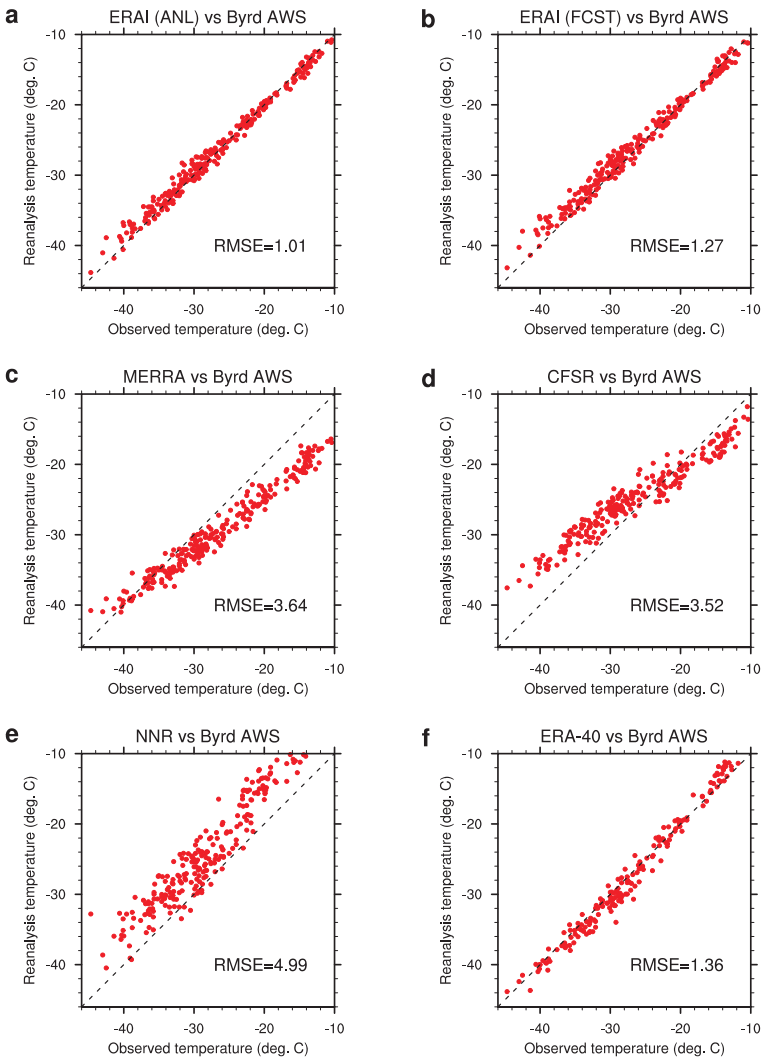

Supplementary Figure S8 | Scatter plots of monthly 2-meter temperature (T_{2m}) estimates from five global reanalyses interpolated to Byrd location (y-axis) versus the observed monthly mean temperatures from Byrd AWS (x-axis). The root mean square error (RMSE) of the reanalysis data with respect to the observations, in units of degrees Celsius, is shown in the bottom-right corner of each plot. The reanalysis datasets are: ERA-Interim (**a**,**b**); MERRA (**c**); CFSR (**d**); the NCEP-NCAR Reanalysis (**e**); and ERA-40 (**f**). For ERA-Interim, separate plots are shown for the *analysis* T_{2m} (**a**) and the *forecast* T_{2m} (**b**). The reanalysis data are adjusted for the model versus observed elevation differences using a dry adiabatic lapse rate of 0.01 °C m^{-1}.

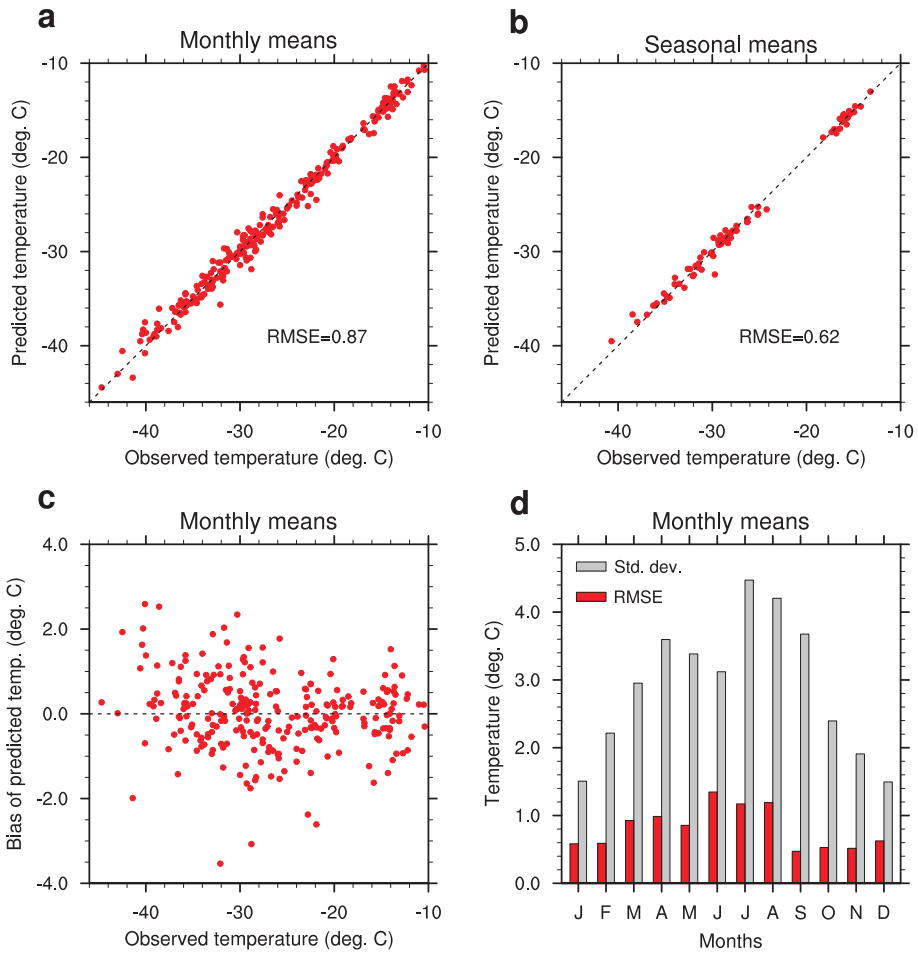

Supplementary Figure S9 | **a**, Scatter plots of the monthly mean temperatures (T_{rec}) predicted by our main infilling method (see main text Methods) (y-axis), versus the observed monthly mean temperatures from Byrd AWS (x-axis). The temperature data are from the time period covered by ERA-Interim (1979-2011). The comparison between predicted and observed temperatures is done only for months with $\geq$90% of observations available. The root mean square error (RMSE) of T_{rec} with respect to the observations is shown in the bottom-right corner of the plot. **b**, Same as **a** but for the seasonal mean temperatures. **c**, Bias of the monthly T_{rec} estimates with respect to the observations (y-axis) as a function of the observed temperature (x-axis). **d**, Histograms comparing the RMSE of T_{rec} (red bars) and the standard deviation of the monthly mean temperatures (gray bars) for each month of the year.

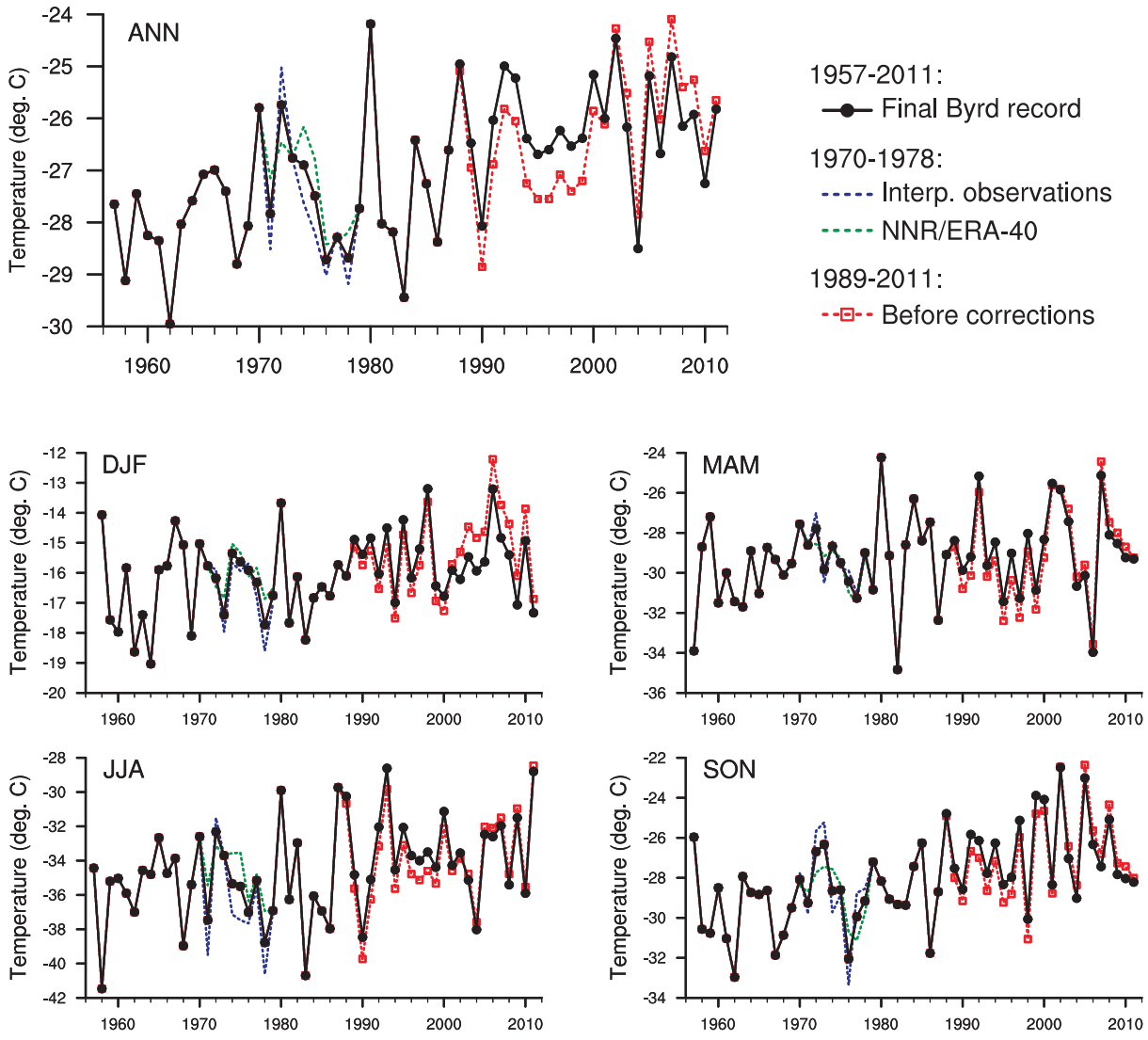

Supplementary Figure S10 | Annual and seasonal mean temperature time series from the final reconstructed Byrd record (black curve) and from the following datasets: interpolated temperature observations from Antarctic research stations (blue curve); adjusted 2-meter temperature estimates from the ERA-40 (for DJF) and NNR (for the other seasons) reanalyses (green curve); reconstructed Byrd record based upon uncorrected AWS observations (red curve). Details about the infilling procedure used for the 1970s and the corrections made to the 1989–01/2011 observations are given, respectively, in the main text Methods and in Supplementary Methods 2.1.

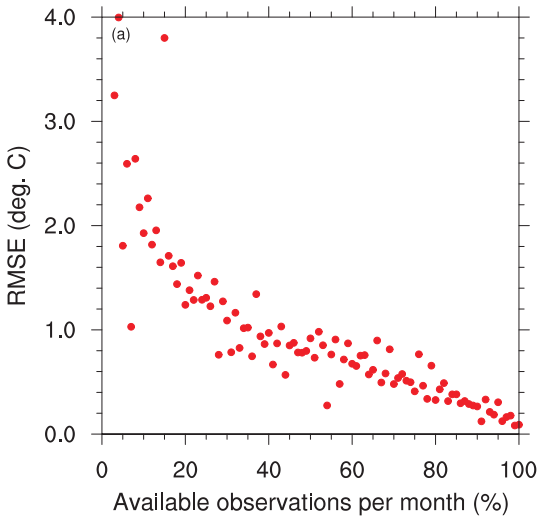

Supplementary Figure S11 | Root mean square error (RMSE) of the monthly mean temperatures predicted by our alternative infilling method (see Supplementary Methods 2.1) (y-axis), as a function of the percentage of 6-hourly observations available per month from the Byrd AWS (x-axis). The percentage of observations available each month is varied through random selection of 6-hourly data. Only the data from 1980–1988 (when the Byrd AWS record is most complete) were used to ensure a uniform sampling of the seasons.

6 Supplementary Tables

Supplementary Table S1 | Linear temperature trends at Byrd computed for: the 1958–2010 and 1980–2010 periods using the fully reconstructed Byrd record (columns 2 and 3); the 1958–2010 period using the reconstructed Byrd record with no infilling of the missing data between 1970 and 1978 (column 4); and the 1958–2010 period using the uncorrected Byrd AWS observations available prior to December 2011 (column 5). As in Fig. 3a,b, the trends represent the averages of those computed between the first three years and last three years of each period. The trend uncertainties are based upon the standard error of the linear regression and the error of the infilling method. Bold (italicized) numbers highlight the trends that are statistically significant at the 95% (90%) confidence level, as estimated from a Student's t-test. The numerical value of the statistical significance is given in brackets.

Season or month	Linear temperature trends (deg. C per decade)			
	1958–2010	1980–2010	1958–2010 (no infill. 1970s)	1958–2010 (uncorrected)
ANN	**0.47±0.23 (99.9)**	*0.51±0.52 (93.1)*	**0.50±0.21 (99.9)**	**0.48±0.25 (99.9)**
DJF	**0.30±0.27 (96.6)**	0.36±0.55 (79.5)	**0.30±0.26 (97.1)**	**0.42±0.27 (99.6)**
MAM	0.24±0.46 (69.7)	0.14±1.09 (20.3)	0.26±0.46 (72.4)	0.23±0.45 (67.1)
JJA	**0.54±0.51 (95.6)**	0.68±1.19 (72.6)	**0.51±0.49 (95.4)**	*0.49±0.51 (93.0)*
SON	**0.82±0.40 (99.9)**	0.85±1.16 (82.6)	**0.85±0.41 (99.9)**	**0.82±0.40 (99.9)**
DJ	**0.45±0.28 (99.7)**	**0.76±0.66 (96.4)**	**0.52±0.24 (99.9)**	**0.55±0.37 (99.2)**
Jan	**0.42±0.30 (99.1)**	*0.60±0.68 (90.4)*	**0.44±0.29 (99.5)**	**0.56±0.40 (98.9)**
Feb	0.18±0.62 (43.6)	0.51±1.73 (42.6)	0.15±0.61 (36.0)	0.26±0.61 (58.2)
Mar	0.48±0.70 (81.6)	1.21±1.66 (82.9)	0.54±0.70 (85.9)	0.52±0.77 (79.8)
Apr	-0.03±0.80 (6.5)	-0.23±1.62 (21.2)	-0.09±0.81 (16.4)	-0.06±0.81 (12.1)
May	0.28±0.66 (58.9)	-0.56±1.55 (51.0)	0.32±0.67 (64.5)	0.23±0.67 (49.4)
Jun	*0.70±0.70 (94.1)*	0.71±1.53 (62.9)	**0.71±0.69 (95.2)**	*0.66±0.70 (92.9)*
Jul	0.52±0.85 (76.4)	0.92±2.12 (59.8)	0.45±0.83 (70.4)	0.47±0.85 (71.4)
Aug	0.40±0.91 (60.4)	0.39±2.05 (28.4)	0.37±0.94 (55.6)	0.33±0.92 (51.2)
Sep	**1.15±0.81 (99.1)**	1.30±1.98 (78.4)	**1.10±0.82 (98.6)**	**1.08±0.82 (98.5)**
Oct	**0.83±0.70 (97.1)**	0.34±1.76 (28.6)	**0.87±0.73 (96.9)**	**0.83±0.72 (96.7)**
Nov	**0.48±0.43 (96.5)**	0.90±1.21 (82.8)	**0.55±0.44 (98.0)**	**0.55±0.46 (97.5)**
Dec	**0.26±0.25 (95.6)**	-0.04±0.60 (9.1)	*0.25±0.25 (94.8)*	**0.40±0.27 (99.3)**

Supplementary Table S2 | Linear temperature trends at Byrd in degrees Celsius per decade from our reconstruction ("This study") and from several other Antarctic temperature datasets: Chapman and Walsh (2007) [ref. 27]; Monaghan *et al.* (2008) [ref. 28]; Steig *et al.* (2009) [ref. 29]; and O'Donnell *et al.* (2010) [ref. 30]. The trends are computed for the 1958–2005 and 1958–2001 periods, respectively, to account for the different time spans of the datasets. As in Fig. 2a,b, the trends represent the averages of those computed between the first three years and last three years of each period. The trend uncertainties are based upon the standard error of the linear regression and (only for our reconstruction) the error of the infilling method. Bold (italicized) numbers highlight the trends that are statistically significant at the 95% (90%) confidence level, as estimated from a Student's t-test.

Period	Season	Linear temperature trends (deg. C per decade)						
		This study	Chapman & W. (2007)[a]	Monaghan *et al.* (2008)[b]	Steig *et al.* (2009)[c]		O'Donnell *et al.* (2010)[d]	
					v1	v2	RLS	E-W
1958 to 2005	ANN	**0.49±0.28**	-	**0.31±0.25**	**0.26±0.24**	0.19±0.23	0.05±0.16	0.02±0.18
	DJF	**0.32±0.31**	-	*0.29±0.30*	0.16±0.22	0.09±0.25	0.05±0.18	0.10±0.21
	MAM	0.26±0.49	-	0.16±0.48	**0.25±0.23**	0.18±0.24	-0.05±0.32	-0.07±0.31
	JJA	*0.49±0.58*	-	0.04±0.61	0.31±0.45	0.24±0.43	-0.05±0.38	-0.10±0.36
	SON	**0.92±0.47**	-	**0.74±0.41**	**0.33±0.30**	**0.26±0.25**	*0.26±0.27*	0.16±0.26
1958 to 2001	ANN	**0.54±0.32**	0.07±0.19	*0.25±0.29*	*0.29±0.29*	**0.27±0.25**	0.05±0.19	0.03±0.22
	DJF	*0.34±0.37*	0.03±0.16	0.16±0.37	0.18±0.26	0.16±0.26	0.05±0.21	0.13±0.25
	MAM	0.28±0.58	0.03±0.38	0.09±0.57	**0.31±0.25**	**0.29±0.25**	-0.05±0.38	-0.06±0.36
	JJA	**0.66±0.66**	0.11±0.47	0.15±0.69	0.42±0.51	0.39±0.46	0.04±0.44	-0.04±0.42
	SON	**0.92±0.47**	0.11±0.30	**0.60±0.45**	0.28±0.38	0.26±0.33	0.19±0.30	0.10±0.31

[a]Temperature data for 1957–2002 are made available by W. Chapman at http://igloo.atmos.uiuc.edu/ANTARCTIC/.

[b]For Monaghan *et al.* (2008), we used the updated version of their reconstructed Byrd temperature record, which is infilled as described in ref. 31. This reconstruction relies on temperature observations from Byrd AWS prior to the 2011 corrections (see Supplementary Discussion).

[c]The dataset, v1, is the main reconstruction from Steig *et al.* (2009) and relies on non-detrended satellite infrared observations. The dataset, v2, is a second reconstruction presented in their supplementary information and using detrended satellite infrared observations. The two temperature datasets (spanning 1957-2006) are made available by E. Steig at http://faculty.washington.edu/steig/nature09data/data/.

[d]The two temperature reconstructions are based, respectively, upon the regularized least square (RLS) and the eigenvector-weighted (E-W) methods presented in the study by O'Donnell *et al*. The 1957–2006 temperature data are made available by R. O'Donnell at http://www.climateaudit.info/data/odonnell/.